Mechanism of Voltage-Dependent Gating in Skeletal Muscle Chloride Channels

Christoph Fahlke,*§ Angela Rosenbohm,* Nenad Mitrovic,# Alfred L. George, Jr.,§¶ and Reinhardt Rüdel*
*Department of General Physiology and #Department of Applied Physiology, University of Ulm, D-89069 Germany, and Departments of §Medicine and ¶Pharmacology, Vanderbilt University Medical Center, Nashville, Tennessee 37232-2372 USA

ABSTRACT Voltage-dependent gating was investigated in a recombinant human skeletal muscle Cl^- channel, hClC-1, heterologously expressed in human embryonic kidney (HEK-293) cells. Gating was found to be mediated by two qualitatively distinct processes. One gating step operates on a microsecond time scale and involves the rapid rearrangement of two identical intramembranous voltage sensors, each consisting of a single titratable residue. The second process occurs on a millisecond time scale and is due to a blocking-unblocking reaction mediated by a cytoplasmic gate that interacts with the ion pore of the channel. These results illustrate a rather simple structural basis for voltage sensing that has evolved in skeletal muscle Cl^- channels and provides evidence for the existence of a cytoplasmic gating mechanism in an anion channel analogous to the "ball and chain" mechanism of voltage-gated cation channels.

INTRODUCTION

Voltage-gated Cl^- channels serve a variety of physiological functions in nearly all cells. In the past, technical problems have prevented a detailed description of their gating properties. With the molecular cloning of the ClC family of voltage-gated Cl^- channels (Jentsch et al., 1990) and the potential for heterologous expression, it is now possible to give a more detailed description of the basic biophysical characteristics of these important ion channels.

The principal Cl^- channel of adult mammalian skeletal muscle (ClC-1) is responsible for the unusually high resting membrane Cl^- conductance characteristic of this tissue (Steinmeyer et al., 1991b). Its physiological importance has recently been underscored by the identification of genetic mutations in the murine and human ClC-1 genes, which cause hereditary disorders of muscle membrane excitability (Steinmeyer et al., 1991a; Koch et al., 1992; George et al., 1993). The resulting condition is called myotonia, a transient muscle stiffness following voluntary contraction, which is caused by a delay in relaxation due to repetitive trains of action potentials.

It has long been recognized that native skeletal muscle Cl^- channels exhibit gating transitions that occur with changing membrane potential (channels activate with depolarization and deactivate upon hyperpolarization) (Warner, 1972; Vaughan et al., 1991; Fahlke and Rüdel, 1995), and identical gating behavior has more recently been demonstrated with recombinant rat and human ClC-1 (Steinmeyer et al., 1991b; Pusch et al., 1994). Despite these descriptions of ClC-1 gating, no coherent biophysical mechanisms have been proposed to explain its behavior. Unlike members of the voltage-gated cation channel gene superfamily, ClC channels lack a structural motif analogous to the S4 helix (Jentsch et al., 1990), which functions as a voltage sensor for the control of gating in voltage-gated Na^+ and K^+ channels (Stühmer et al., 1989; Papazian et al., 1991). Although mechanisms involved in the gating of the *Torpedo electroplax* Cl^- channel (ClC-0) have been elucidated in part (White and Miller, 1979; Hanke and Miller, 1983; Richard and Miller, 1990; Pusch et al., 1995), little is known about the voltage-dependent gating of mammalian ClC Cl^- channels. Recently we examined the functional characteristics of a missense mutation affecting an aspartic acid residue at position 136 of human ClC-1 (hClC-1) that causes the recessive form of myotonia congenita (Fahlke et al., 1995). This mutation greatly affects voltage-dependent gating of the channel without causing dramatic changes in chloride permeation, suggesting that the gating mechanism of hClC-1 involves a voltage sensor. Using the whole-cell patch-clamp recording technique, we have studied a recombinant hClC-1 in greater detail and propose a model to explain the gating of this channel.

MATERIALS AND METHODS

Stable expression of hClC-1 in HEK-293 cells

HEK-293 cells (ATCC CRL 1573) were transfected by the calcium phosphate precipitation method (Graham and van der Eb, 1973), using the plasmid pRc/CMV-hClC-1 as previously described (Fahlke et al., 1995). Oligoclonal cell lines were obtained by selection for resistance to the aminoglycoside antibiotic Geneticin (G418; Boehringer Mannheim, Germany). Twenty hours after transfection, cells were incubated in medium supplemented with G418 (800 μg/ml). After 10–28 days, G418-resistant foci were picked and plated in individual flasks. The cells were then electrophysiologically tested after 3–6 days in culture. Cell lines in which more than three consecutively tested cells did not show current amplitudes of >300 pA at −135 mV were classified as negative. Six of the 11 cell lines were positive, and three were kept in culture for >18 months. For

Received for publication 29 September 1995 and in final form 1 May 1996.

Address reprint requests to Dr. Alfred L. George, Jr., S-3223 MCN, Vanderbilt University Medical Center, 21st Avenue South at Garland, Nashville, TN 37232-2372. Tel.: 615-343-1168; Fax: 615-343-7156; E-mail: ageorge@mbio.mc.vanderbilt.edu.

Dr. Fahlke's present address is S-3223 MCN, Vanderbilt University Medical Center, Nashville, TN 37232-2372.

0006-3495/96/08/695/12 $2.00

control experiments measuring the contribution of endogenous Cl^- currents, nontransfected HEK 293 cells were cultured in media without G418 under identical conditions.

Electrophysiology

Standard whole-cell recording (Hamill et al., 1981) was performed using an EPC-7 (List, Darmstadt, Germany) or an Axopatch 200A amplifier (Axon Instruments, Foster City, CA). Pipettes were pulled from borosilicate glass and had resistances of 0.5–1.0 MΩ. Currents were filtered with the internal filters of the amplifiers and were recorded using a Digidata 1200 AD/DA converter (Axon Instruments). The sampling frequencies (between 5 and 333 kHz) were at least three times larger than the filtering frequency. The time between test sweeps was at least 15 s. Because the open probability of hClC-1 is different from zero over the entire voltage range between −200 and +150 mV, it is not possible to use leakage or capacitance subtraction. Digital subtraction of leakage and capacitive current was therefore not applied.

Current responses to 10-mV voltage steps from a holding potential of 0 mV in the positive direction were fit with a single exponential time course to obtain the charging time constant, the series resistance, and the cell capacitance. The average charging time constant was 20 ± 18 μs (n = 6). The average cell capacitance was 30 ± 5 pF (n = 6). More than 60% of the series resistance was compensated by an analog procedure. The calculated voltage error due to series resistance was always less than 5 mV.

To obtain different Cl^- gradients, three different pipette solutions were used (all concentrations in mM): 1) 130 CsCl, 2 $MgCl_2$, 5 EGTA, 10 HEPES (standard internal solution); 2) 50 CsCl, 80 $CsCH_3SO_3$, 2 $MgCl_2$, 5 EGTA 10 HEPES; or 3) 10 CsCl, 120 $CsCH_3SO_3$, 2 $MgCl_2$, 5 EGTA 10 HEPES. The bathing solution contained 1) 140 NaCl, 4 KCl, 2 $CaCl_2$, 1 $MgCl_2$, and 5 HEPES (standard external solution); 2) 70 NaCl, 70 $NaCH_3SO_3$, 4 KCl, 2 $CaCl_2$, 1 $MgCl_2$, 5 HEPES; 3) 35 NaCl, 105 $NaCH_3SO_3$, 4 KCl, 2 $CaCl_2$, 1 $MgCl_2$, 5 HEPES; or 4) 10 NaCl, 130 $NaCH_3SO_3$, 4 KCl, 2 $CaCl_2$, 1 $MgCl_2$, 5 HEPES. Solutions were adjusted to the desired pH with CsOH (pipette solutions) or NaOH (bath solutions). For the variation in pH_i or pH_e, HEPES was substituted on an equimolar basis with 2-(*N*-morpholino)ethanesulfonic acid (MES) for pH 5.4–6.7, and with (3-[1,1-dimethyl-2-hydroxyethyl)amino]-2-hydroxypropane-sulfonic acid (AMPSO) for pH 8.3–9.5. Standard solutions were used unless otherwise stated. Agar bridges (3 M KCl in 0.1% agar) were used to connect solutions with the amplifier in experiments with large Cl^- gradients.

Data analysis

Data were analyzed by a combination of pClamp (Axon Instruments) and SigmaPlot (Jandel Scientific, San Rafael, CA) programs. Unless otherwise noted, all data are shown as means ± SD.

For the description of the time course of current activation or deactivation, a sum of two exponentials and a time-independent value (d) were fitted to the data: $I(t) = a_1\exp(-t/\tau_1) + a_2\exp(-t/\tau_2) + d$. The relative components of current deactivation were calculated by dividing the individual records by the peak current amplitude (I_{max}) determined after a long (>500 ms) prepulse to +55 mV: $A_1 = a_1/I_{max}$, $A_2 = a_2/I_{max}$, $C = d/I_{max}$. The relative components of current activation were calculated as $A_1 = -a_1/I_{max}$, $A_2 = -a_2/I_{max}$, $C = d/I_{max}$. Activation was analyzed for negative membrane potentials only. "Instantaneous" current amplitudes were determined 200 μs after the voltage step.

To obtain the voltage dependence of activation, the instantaneous current amplitude at a fixed potential of −135 mV was measured after prepulses to different voltages (V) and divided by its maximum value. The normalized data were then plotted versus the preceding potential as described previously (Fahlke et al., 1995). This plot yields the voltage dependence of the relative open probability, P_{open}, at the end of the prepulse. The steady-state activation curve was obtained by using 1.4-s prepulses. Steady-state activation curves obtained in this manner were fitted with a single Boltzmann term and a voltage-independent value: $I(V) = \text{Amp} \cdot [1 + \exp([V - V_{0.5}]/k_V)]^{-1} + \text{constant}$.

RESULTS

Gating Behavior of hClC-1

Fig. 1 *A* shows representative whole-cell currents recorded from a cell that stably expresses hClC-1. The voltage steps start from a holding potential of −30 mV. During depolarizing voltage steps, the currents are time independent. During hyperpolarizing steps, the currents increase instantaneously and then rapidly deactivate to a nonzero steady-state level. The time-dependent channel gating responsible for this deactivation is further illustrated by a plot of the amplitudes of the instantaneous and the steady-state currents versus membrane potential (Fig. 1 *B*).

The contribution of endogenous currents to the recordings illustrated in Fig. 1 *A* was estimated by the repetition of these experiments with nontransfected HEK 293 cells cultured under identical conditions. Whole-cell currents from these cells were very small and time independent (Fig. 1, *C* and *D*). These experiments illustrate that, under our experimental conditions, all currents are carried by hClC-1 channels, and contributions of endogenous or leakage currents are negligible.

The time course of deactivation in current transients as shown in Fig. 1 *A* was best fit with two exponentials plus a time-independent term (see Materials and Methods), thus resolving the expressed currents into three distinct components: fast deactivating, slow deactivating, and nondeactivating. A quantitative description of the gating of hClC-1 is given by the time constants τ_1 and τ_2 for fast and slow gating, respectively (Fig. 1 *E*), and by a plot of the voltage dependencies of the fractional amplitudes of the three components (Fig. 1 *E*). The latter were obtained by dividing each set of fitted amplitudes by the respective instantaneous current amplitudes recorded after a prepulse to +55 mV, a potential at which channels are maximally activated. At this potential, the instantaneous current amplitude represents the product of the single-channel amplitude times the number of channels times the maximum open probability. Therefore, for each test potential, the calculated fractional current amplitudes represent the percentages of channels in the fast, slow, or time-independent gating state times the relative open probability at the holding potential of −30 mV. Because at −30 mV activation of the channels is not at its maximum, the sum of the calculated fractional current amplitudes is smaller than unity.

The voltage dependences exhibited by the deactivation time constants and the fractional amplitudes are very different. Both the time constants for fast and slow deactivation are voltage independent (Fig. 1 *E*), whereas each of the fractional current amplitudes has its own characteristic potential dependence (Fig. 1 *F*): as the test potential is varied from −195 to −45 mV, the fast deactivating component (A_1) decreases, the nondeactivating component (C) in-

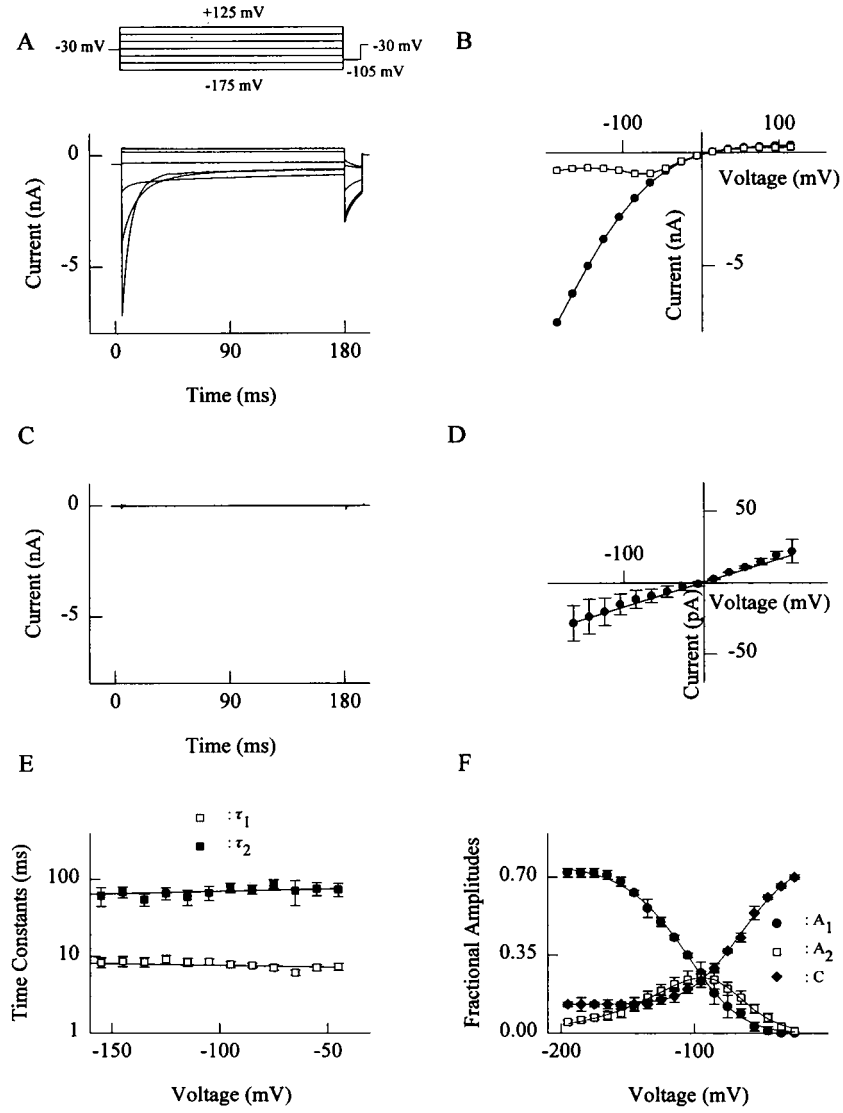

FIGURE 1 Deactivation of hClC-1 Cl^- currents in stably transfected HEK 293 cells recorded under standard conditions (internal solution, in mM: 130 CsCl, 2 $MgCl_2$, 5 EGTA, 10 HEPES, pH 7.4; bathing solution, in mM: 140 NaCl, 4 KCl, 2 $CaCl_2$, 1 $MgCl_2$, and 5 HEPES, pH 7.4). (*A*) Current responses to voltage steps from a holding potential of −30 mV into the range between −175 mV and +125 mV. Each test pulse is followed by a fixed voltage step to −105 mV. (*B*) Voltage dependence of the current amplitudes at the beginning (●) and end (○) of responses. The two axes intersect at zero. Data from the experiment shown in *A*. (*C*) Current responses of a nontransfected HEK 293 cell to the pulse protocol shown in *A*. (*D*) Voltage dependence of current amplitudes measured at the beginning of test pulses on nontransfected HEK 293 cells. Each data point represents the mean ± SD from six cells. A regression line with a slope of 0.16 nS ($r^2 = 0.98$) is fitted to the data points. (*E*) Voltage dependence of the deactivation time constants obtained from biexponential fits. (*F*) Voltage dependence of amplitudes of the three current components (A_1, fast deactivating; A_2, slow deactivating; *C*, nondeactivating). Solid lines represent fits of the data with Boltzmann functions as described in the text. Data in *E* and *F* are means ± SEM from at least seven cells.

creases, and the slow deactivating component (A_2) increases and then decreases (i.e., is bell-shaped). The voltage dependence of the fast deactivating component could be fitted with $(B_1)^2$, that of the nondeactivating component with $(1 - B_2)^2$, and that of the slowly deactivating component with $2 \cdot B_3(1 - B_4)$, where $B_i = [1 + \exp([V - V_{0.5,i}]/k_{V,i})]^{-1}$ (the rationale for these fits is provided in the next section). An examination of Boltzmann parameters derived from these data fits (Table 1) reveals that they are for the most part not statistically different for the three current components. This suggests that there exists a binomial distribution of channels exhibiting fast, slow, or nondeactivating behavior.

Currents with activating kinetics are elicited during depolarizing voltage steps when the test pulses are preceded by a conditioning potential of −85 mV. The time course of activation can also be well fitted with the sum of two exponentials and a constant term. As observed for deactivation, the time constants of activation are voltage independent (at negative potentials). The fast activation time constants are almost indistinguishable from those of deactivation (Fig. 2C). Like deactivation, the component amplitudes of activation display voltage dependencies that are qualitatively similar to that of deactivation within the tested voltage range for activation (Fig. 2 *D*).

TABLE 1 Boltzmann parameters derived for voltage-dependent fractional current amplitudes

Component*	Amplitude	Boltzmann term	
		$V_{0.5}$ (mV)	k_V (mV)
Fast deactivating	0.74 ± 0.13	−86.0 ± 11.1	29.1 ± 2.9
Nondeactivating	0.68 ± 0.14	−91.6 ± 17.1	23.9 ± 5.7
Slow deactivating	0.73 ± 0.3	−85.5 ± 20.5	13.4 ± 1.4
		−103.7 ± 30.2	27.2 ± 2.6

*Fractional current amplitudes were fit with the following Boltzmann functions: fast deactivating, $Amp(B_1)^2$; slow deactivating, $Amp[2 \cdot B_3(1 - B_4)]$; nondeactivating, $Amp(1 - B_2)^2$, where *Amp* is the component amplitude and $B_i = [1 + \exp([V - V_{0.5,i}]/k_{V,i})]^{-1}$.

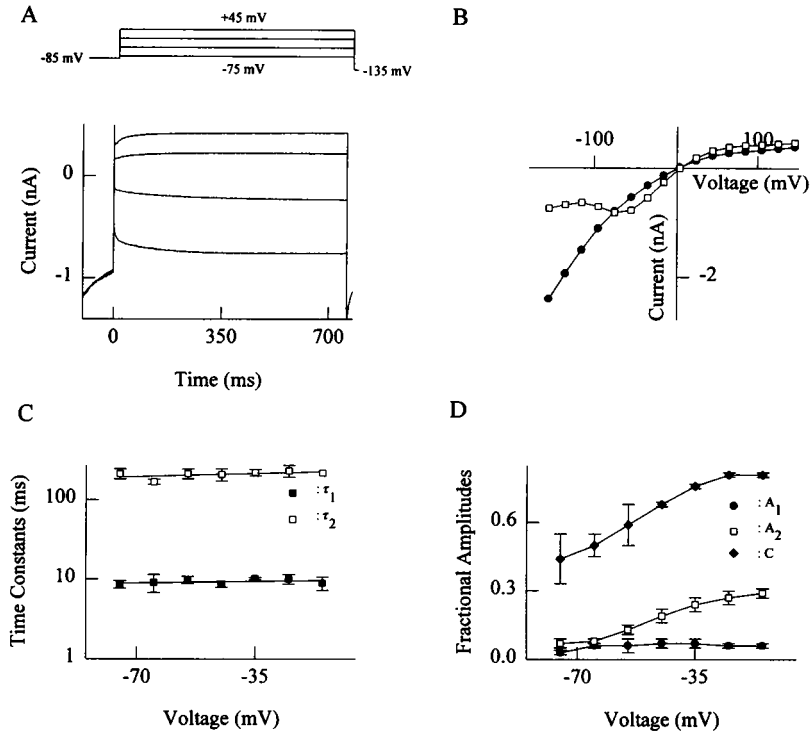

FIGURE 2 Activation of hClC-1 Cl^- currents. (*A*) Current responses to voltage steps between −75 mV and +45 mV after a depolarizing prepulse to −85 mV. Each test pulse is followed by a fixed voltage step to −135 mV. (*B*) Voltage dependence of the current amplitudes measured at the beginning (●) and at the end of test pulses. Data were obtained from the same experiment as shown in *A*. (*C*) Voltage dependence of the activation time constants obtained from biexponential fits from at least four cells. (*D*) Voltage dependence of fractional current amplitude (A_1, fast activating fraction; A_2, slow activating fraction; *C*, instantaneous current). Data in *C* and *D* are means ± SD from at least four cells.

Gating model for hClC-1

As a consequence of the described voltage independence of the time constants, the voltage dependence of the current components, and the similarity between activation and deactivation time constants, gating of hClC-1 cannot be appropriately represented by a sequential state model. In sequential models, the voltage dependencies of fractional current amplitudes are determined by the voltage dependencies of the rate constants connecting different states (Brown et al., 1983; Chiu, 1977). Our results are more consistent with the assumption that two distinct processes are involved in gating: 1) a voltage-sensing process governing the distribution of channels among the three distinct kinetic states (fast deactivating, slow deactivating, and nondeactivating) and 2) another mechanism mediating the voltage-independent opening and closing of the channel.

The simplest model designed to account for the voltage dependence of the three current components (Fig. 3) contains a set of two identical voltage sensors, each of which may assume one of two possible positions (↑ and ↓). This leads to four possible configurations (↑ ↑, ↑ ↓, ↓ ↑, ↓ ↓), two of which (↑ ↓, ↓ ↑) exert equivalent effects on channel function and therefore are indistinguishable. The voltage dependence of the probability of one voltage sensor being in one position is given by a simple Boltzmann distribution. The distribution of the positions of two identical voltage sensors over the three configurations (↑ ↑, [↑ ↓, ↓ ↑], ↓ ↓) is therefore given by a binomial function of the Boltzmann terms B and $1 - B$. We therefore expect that the voltage dependence of ↑ ↑ is given by B^2; that of [↑ ↓, ↓ ↑] by $2B^*(1 - B)$; and that of ↓ ↓ by $(1 - B)^2$. This mathematical description matches perfectly the observed voltage dependence of each of the three distinct kinetic states (Fig. 1 *F*).

Therefore, we suggest that the three experimentally observed kinetic states correspond to three different channel conformations depicted in Fig. 3. In this arrangement, movements of the voltage sensors determine whether channel deactivation is fast or slow or does not occur at all. These voltage sensor movements must occur very rapidly, so that the distribution of channels among the three kinetic states achieves equilibrium before the process of opening or closing begins. We further suggest that the time-dependent channel closing and opening transitions are mediated by a structurally different mechanism (distinct from voltage-sensor movements) that has no intrinsic voltage dependence (Fig. 3).

In the following, evidence will be presented in support of the basic concepts of this model. This will include 1) demonstrating the existence of very rapid gating steps, 2) showing that it is possible to dissociate changes in the fractional current amplitudes from alterations of the time constants, and 3) providing evidence that the time courses of activation and deactivation can be represented as a blocking-unblocking reaction of the channel with a cytoplasmic gate.

Ultrafast gating in hClC-1

As stated above, it is necessary to propose that the voltage sensors undergo very rapid movements on a time scale much faster than the time course of deactivation and acti-

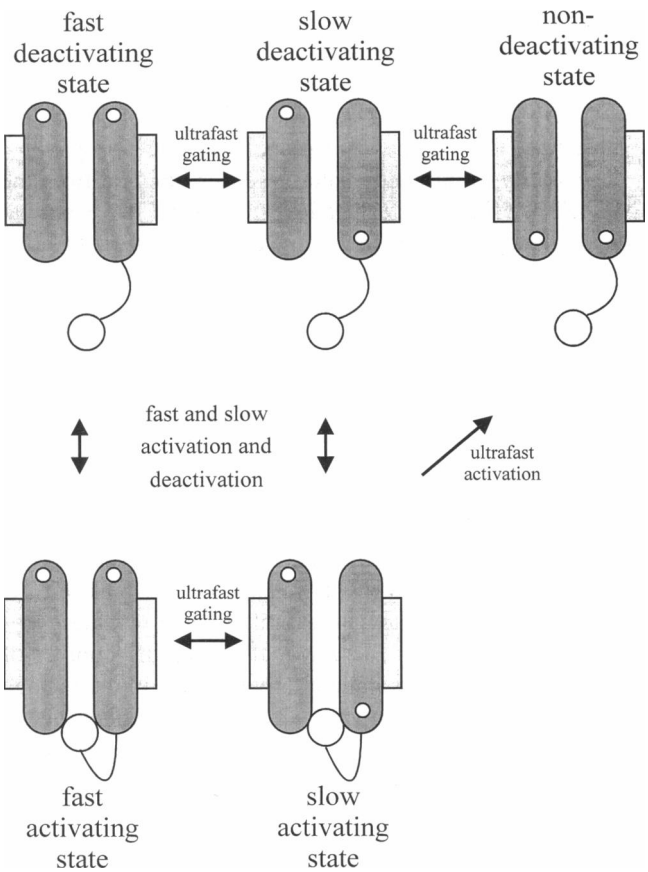

FIGURE 3 Gating model of hClC-1. The hClC-1 channel is represented by two shaded structures, each with a single voltage sensor indicated by a white circle. Independent movements of the voltage sensors between two possible positions (shown as either up or down) occur very rapidly (horizontal "ultrafast" gating steps). The final configuration of voltage sensors then determines the kinetic state of the channel. Transitions between the open and closed channel occur vertically in the model.

vation to explain the basic kinetic features of hClC-1 gating (voltage-independent activation and deactivation time constants and highly voltage-dependent fractional current amplitudes).

The existence of ultrafast gating steps was initially suspected based on the voltage dependence of the instantaneous current amplitude recorded after two different prepulse potentials (−85 mV, −30 mV; Fig. 4 *A*). The instantaneous current flowing after a voltage step is determined by the product of the single-channel current amplitude times the number of open channels. If the number of open channels does not change during the voltage step, the instantaneous current-voltage relationship is determined by the number of open channels at the membrane potential preceding the voltage step. Thus, if such instantaneous current-voltage relationships are determined with two different prepotentials, then the ratio of the two current amplitudes should be independent of the test potential and should equal the ratio of the open probabilities determined for the two prepotentials. When such an experiment was

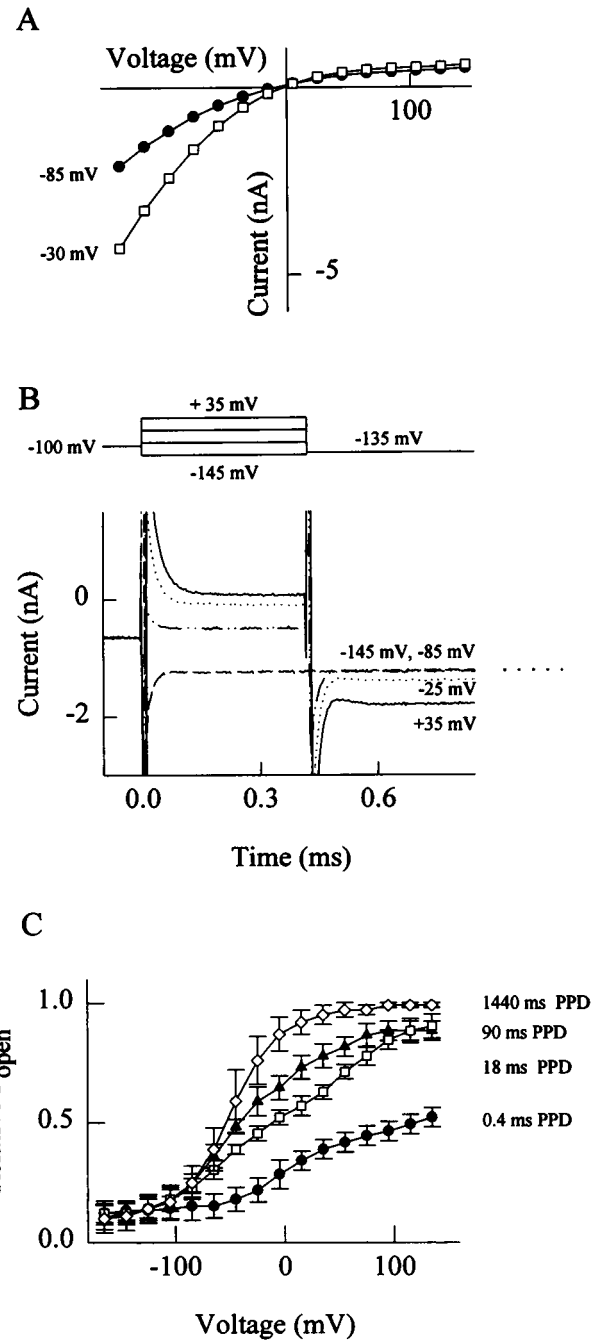

FIGURE 4 Ultrafast steps in the voltage-dependent activation of hClC-1 channels. (*A*) Instantaneous current-voltage relationship from one cell measured after a 155-ms prepulse to either −85 mV (●) or −30 mV (□). (*B*) Current responses to a pulse protocol consisting of a 546-ms conditioning pulse to −100 mV, a 0.4-ms variable prepotential, and a constant test pulse to −135 mV. The dotted line shows the steady-state current amplitude at the −135-mV test pulse 200 ms after the voltage step, which was identical for both prepulses. (*C*) Voltage dependence of the relative open probabilities after 0.4-ms, 18-ms, 90-ms, or 1440-ms prepulses. Data shown are means ± SD (n = 4).

performed with prepotentials of −85 and −30 mV, the instantaneous current amplitudes were different at negative test potentials, but became more similar as the test potential

was made more positive. This indicates that the number of open channels must have changed during the brief time required to charge the membrane for each voltage step. This observation is in agreement with our assumption of an ultrafast gating process.

The ultrafast gating steps can also be investigated by determining the voltage dependence of activation with very short prepulses. In these experiments, the membrane potential was first held for 546 ms at −100 mV to achieve current deactivation, then prepulses of 0.4 ms duration and varying voltage were applied, followed by a fixed test pulse to −135 mV. The instantaneous current amplitude (and, by inference, the number of open channels) increased with more positive prepulse potentials (Fig. 4 *B*, pulses to −25 or +35 mV). The lack of any visible change in the current amplitude during the prepulse supports the notion that an ultrafast gating process is taking place during the capacitative transient. Ultrafast gating steps only take place upon membrane depolarization (channel activation), and a deactivating ultrafast process does not seem to exist.

When activation curves were determined using various prepulse durations, the voltage dependence and the maximum value of the open probability changed (Fig. 4 *C*). P_{open} reached a steady-state value when the prepulse duration was as long as 1440 ms; longer prepulse durations do not further change the maximum value of P_{open}. Comparison of the current amplitudes reached with prepulses of 0.4 ms and 1440 ms shows that about 50% of the maximum P_{open} is already obtained after a very short time (Fig. 4 *C*).

Titration of hClC-1 voltage sensors by variation of the external pH

The gating of skeletal muscle Cl^- channels has long been known to vary with external pH (pH_e) (Vaughan et al., 1991; Warner, 1972). We chose to probe the chemical nature of the gating mechanisms by varying pH_e and to attempt to dissociate effects on the two proposed gating processes.

Fig. 5 *A* shows current responses to voltage steps from −30 mV to −145 mV and +45 mV recorded from a single cell at pH_e = 6.5, 7.4, and 8.5. Only the responses to hyperpolarization were dependent on pH_e, the largest effect being the increased current at pH 6.5. Changes in pH_e had no effect on the time constants of deactivation (Fig. 5 *B*), suggesting that the mechanism directly responsible for channel closing does not involve titratable residues on the extracellular side. By contrast, changes in pH_e have dramatic effects on the relative proportions of the fast (A_1), slow (A_2), and nondeactivating (*C*) current components. External acidification nearly abolishes the voltage dependence of both the fast-deactivating (A_1, Fig. 5 *C*) and nondeactivating current (*C*, Fig. 5 *E*) component amplitudes, whereas the slow-deactivating component (A_2, Fig. 5 *D*) changes from its characteristic bell shape into a monotonic decrease with increasing depolarization. These results show that the voltage-sensing structures within the channel can be titrated from the extracellular side, and that it is possible to dissociate changes in fractional amplitudes from the deactivation time course. The latter is support for the existence of two independent processes in hClC-1 gating.

The ability to influence voltage-sensor function from the extracellular side was further investigated by the examination of steady-state channel activation. For three different pH_e values, the voltage dependencies of relative P_{open} under steady-state conditions were determined and fitted with the sum of a Boltzmann distribution and a constant term (Fig. 5). The slope factor (k_V) derived from these data fits provides an estimate of the equivalent gating charge for each experimental condition. External acidification did not affect this parameter (k_V = 20.1 ± 0.6 mV at pH 6.5; k_V = 20.2 ± 0.9 mV at pH 7.4; k_V = 20.0 ± 1.4 mV at pH 8.5; n = 4), but rather caused an increase in the constant term. An explanation for this effect is that each voltage sensor consists of only a single titratable residue (see Discussion). If the voltage sensor possesses several charged residues, protonation of a subset of these would reduce the number of gating charges, causing a quantitative change in the voltage dependence of activation (i.e., a reduction in slope of the activation curve) (Almers, 1978; Liman et al., 1991; Logothetis et al., 1992), but all channels will still respond to voltage in a qualitative fashion.

Based on the idea that each voltage sensor consists of a single titratable residue, we determined the number of voltage sensors per channel from a titration experiment in which we plotted the fraction of voltage-dependent channels against pH_e (Fig. 6, *A* and *B*). The number of titratable sites involved in voltage sensing and their chemical nature (pK_a) can be discerned from this relationship by applying the Hill equation. The fraction of voltage-dependent channels (defined as the value u) was calculated from the voltage dependence of the nondeactivating current fraction *C*. As defined above, *C* represents the fraction of hClC-1 channels that do not deactivate upon hyperpolarization. We measured the fraction of voltage-dependent channels as the proportion of *C* that changes over the entire range of test potentials (see Fig. 5 *D*). This proportion was obtained by fitting the data in Fig. 4 *D* with the equation $C = k/[1 - (1 + \exp[(V - V_{0.5})/k_V])^{-1}]^2 + c$, and then for different pH_e values, u was calculated as $k/(k + c)$. The dependence of u on pH_e provides an estimate of the pK_a of the involved residues (6.0) and the minimum number of protonation sites per channel (1.7) by fitting a Hill equation to the data (Fig. 7, *A* and *B*).

Evidence for a cytoplasmic gate in hClC-1

Next we examined the effect of internal pH (pH_i) on hClC-1 gating. Unlike pH_e, changes in pH_i had profound effects on the time constants of deactivation and activation. Fig. 8, *A* and *B*, illustrates the effect of pH_i on the time course of deactivation and activation, respectively. Both processes are

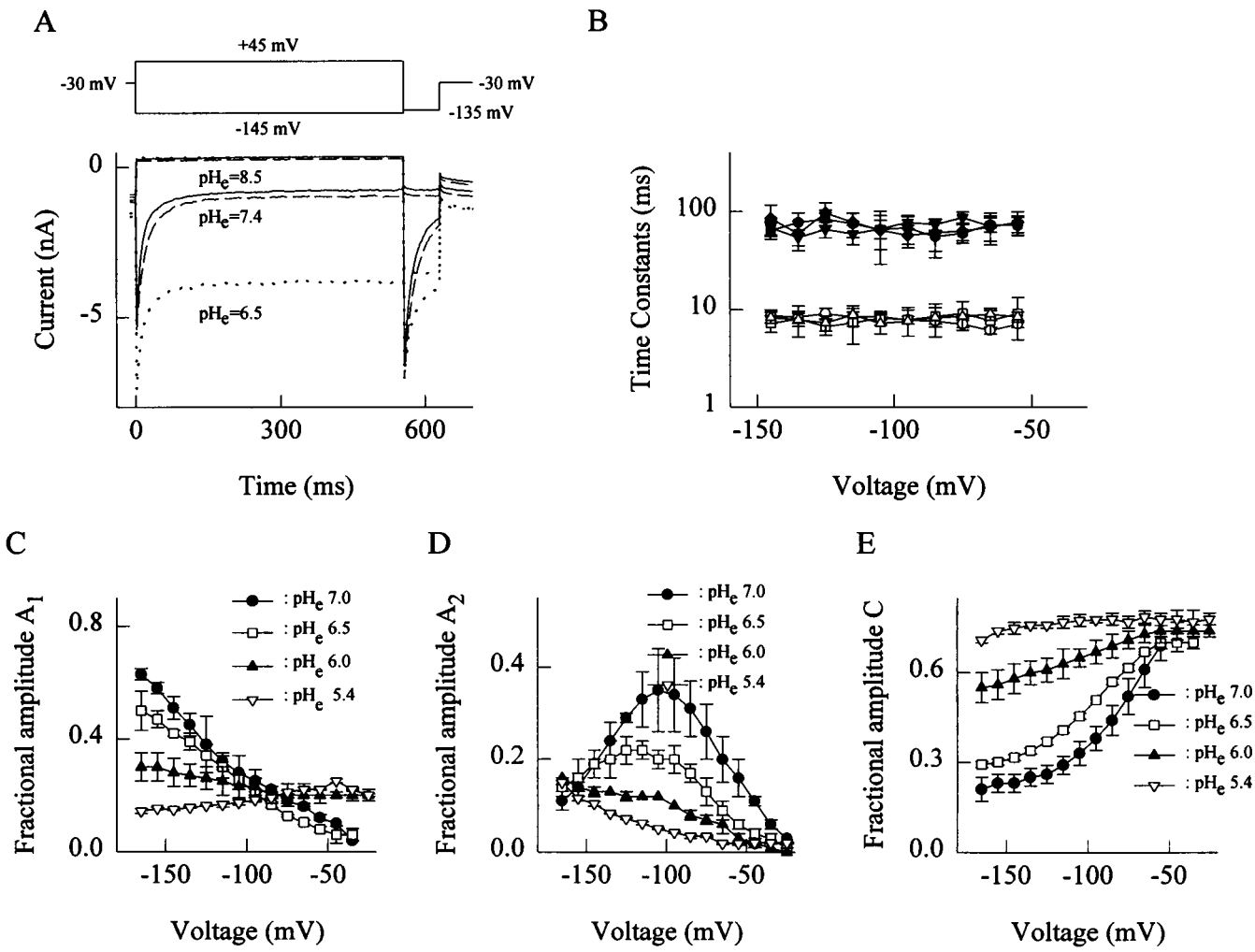

FIGURE 5 External pH affects the hClC-1 voltage sensor. (*A*) Voltage steps to −135 mV and +45 mV obtained from one cell at three different external pHs. Each pulse is followed by a constant test pulse to −125 mV. (*B*) Voltage dependence of the fast (open symbols) and the slow (filled symbols) deactivation time constant for pH_e 6.5 (triangles), 7.4 (circles), 8.5 (squares). Each point represents the mean ± SD from at least four different cells. (*C, D, E*) Voltage dependence of the fractional current amplitudes A1 (*B*), A2 (*C*), and C (*D*) for four different pH_e values obtained from voltage steps from a holding potential of +55 mV. Each point represents the mean ± SD from four different cells.

slowed dramatically by acidic pH_i and are slightly accelerated by alkaline pH_i. For all tested pH_i values, the time constants for fast and slow activation and deactivation remained voltage independent. The fast time constants (τ_{a1}, τ_{d1}) are identical across a wide pH_i range. The slow time constants (τ_{a2}, τ_{d2}) are slightly different but exhibit a similar pH_i dependence (Fig. 8 *C*). The results shown in Fig. 8 *C* are not simple titration curves, suggesting that several titratable groups are involved.

To test for possible effects of permeating ion concentration on the time course of activation and deactivation, similar experiments were performed at various internal and external Cl^- concentrations. The time constants for deactivation as well as the fraction of nondeactivating current depend on the intracellular as well as the extracellular Cl^- concentrations. When plotted versus the calculated Cl^- equilibrium potential (E_{Cl}), the fast and slow deactivation time constants increase with more positive E_{Cl} (Fig. 8 *D*). The fraction of nondeactivating current (I_{ss}/I_{peak}) at very negative potentials increases with either an increasing intracellular Cl^- concentration or a decreasing extracellular Cl^- concentration (Fig. 8 *E*).

These properties of hClC-1 gating are consistent with a blocking and unblocking reaction mediated by a cytoplasmic "gate" (Armstrong and Bezanilla, 1977; Hoshi et al., 1990; Demo and Yellen, 1991). The large effect of varying pH_i on the time constants, their voltage independence at any pH_i, and the absence of any effect of external pH is most consistent with the existence of a cytoplasmic blocking particle composed of titratable residues. Because time constants are affected by the concentration of the permeating ion on both sides of the membrane, we postulate that the blocking particle is directly interacting with the ion-conducting part of the channel, such that this proposed "gate" behaves as an open channel blocker (MacKinnon and Miller, 1988).

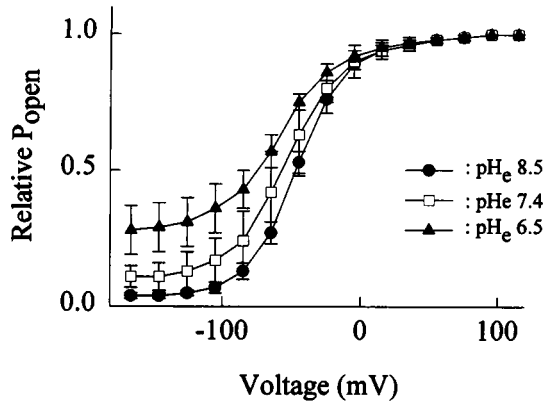

FIGURE 6 Voltage dependence of the steady-state open probability of hClC-1 for three different pH_e values. To construct these activation curves, the instantaneous current amplitude divided by its maximum value at a fixed potential of −135 mV measured after 1.4-s prepulses to different voltages (V) was plotted versus the preceding potential. Each point represents mean data ± SD from four cells. Lines represent fits with a single Boltzmann and a voltage-independent value: $I(V) = \text{Amp} \cdot [1 + \exp([V - V_{0.5}]/k_V)]^{-1} + \text{constant}$.

Because the time constants for fast activation and deactivation are identical within the tested pH_i range (Fig. 8 *C*), we have modeled this gating reaction as a simple first-order process, fully described by a set of two rate constants, k_{on} and k_{off}. We reasoned that if the measurable fast activation and deactivation processes were due to transitions between one closed and one open state,

$$\text{closed} \underset{k_{on}}{\overset{k_{off}}{\rightleftharpoons}} \text{open},$$

then the observed activation and deactivation time constants could both be calculated as $\tau = 1/(k_{on} + k_{off})$ and should therefore be equal. If during fast activation or deactivation more than two different states were involved, the two time constants would be different. At very negative potentials where A_2 and C reach minimum values, the ratio of steady-state to peak current (I_{ss}/I_{peak}) is expected to equal $k_{off}/(k_{on} + k_{off})$. Therefore, the two values τ and I_{ss}/I_{peak} fully determine k_{on} and k_{off}. Variation of the Cl^- gradient specifically changes k_{on} but does not affect k_{off} (Fig. 8 *F*). These observations are consistent with the idea that the cytoplasmic gate is competing with Cl^- ions for a binding site within the pore (MacKinnon and Miller, 1988). Because the rate constant k_{off} does not vary with the Cl^- concentration, it appears that once bound, the gate cannot be easily displaced by the permeating ion.

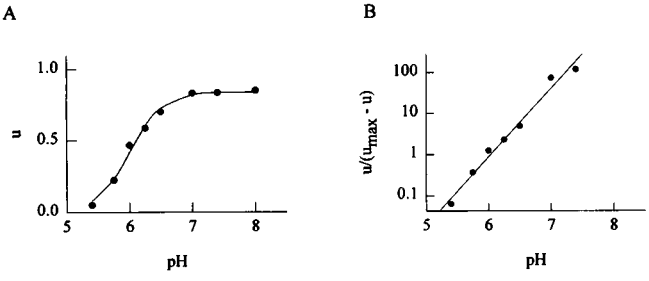

FIGURE 7 Determination of pK_a and minimum number of residues titratable by external pH. (*A*) Dependence of the value u (see text for explanation) on the pH_e. The line represents the best fit of a Hill relationship, $u = u_{max}([H^+]^n/([H^+]^n + K_a^n))$, yielding $n = 1.7$ and $pK_a = 6.0$. (*B*) Transformation of the data by $u/(u_{max} - u)$ and plotting on a logarithmic scale. The regression line shown has a slope of 1.7 ($r^2 = 0.96$).

DISCUSSION

An essential step in understanding the function of ion channels is the development of biophysical models that represent the experimentally determined channel behavior in qualitative and quantitative terms. Such models are extremely valuable for the analysis of the relationship between channel structure and function. After the molecular cloning of at least six different mammalian ClC Cl^- channel isoforms (Steinmeyer et al., 1991b; Thiemann et al., 1992; Uchida et al., 1993; Adachi et al., 1994; Kawasaki et al., 1994; van Siegtenhorst et al., 1994), and the descriptions of some functional properties for a subset of these channels, biophysical models are now necessary as a basis for the understanding of the properties exhibited by this new ion channel family.

The work presented here attempts to understand the molecular basis for gating of the human skeletal muscle voltage-gated Cl^- channel, hClC-1. Our results suggest that two structurally distinct parts of the channel are involved in its gating: a pair of identical voltage sensors, and a cytoplasmic gate that interacts directly with the ion pore. In our proposed model of gating, voltage-dependent movements of the voltage sensors induce rapid changes in the rate constants for the interaction between the cytoplasmic gate and the channel.

Voltage sensors in hClC-1

Considering the profound effect that external pH has on the distribution of channels among the three kinetic states (Fig. 5), we reasoned that the ability of the channel to sense voltage is controlled by titratable residues. Lowering pH_e increased the proportion of channels in the nondeactivating state without affecting the slope factor (k_V) derived from fits of activation curves with the Boltzmann distribution. The identity of the slope factors k_V at three different pH_e values points to a voltage sensor consisting of a single titratable residue. Protonation of this single residue reduces the charge of the voltage sensor to zero and completely abolishes its voltage-sensing ability (i.e., the channel is converted to a nondeactivating pore). In this case, a fraction of channels have fully charged voltage sensors at pH_e 6.5, and their equivalent gating charge is identical to that determined at neutral or alkaline pH_e. The remaining protonated chan-

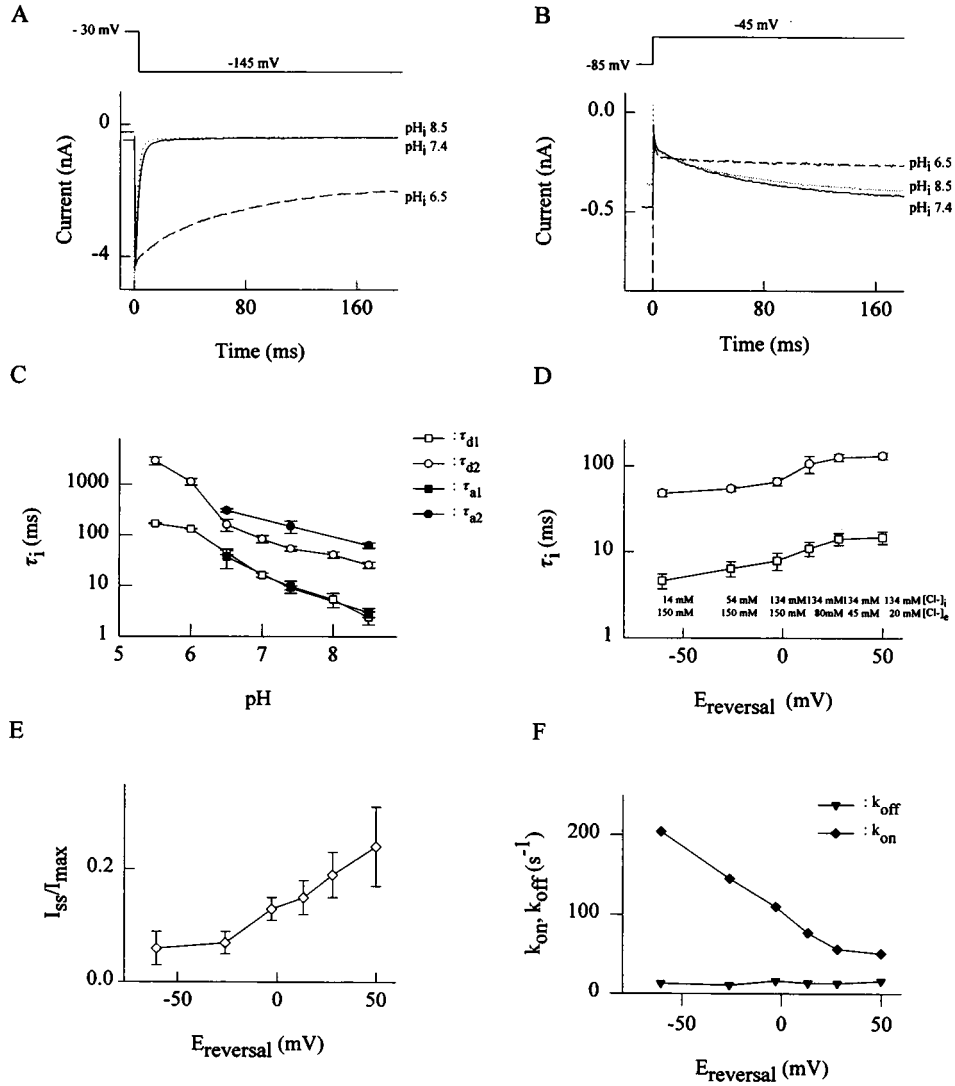

FIGURE 8 Dependence of gating properties on pH_i. (*A*) Current responses to a voltage step to −145 mV from a holding potential of −30 mV recorded from three different cells using pipette solutions with pH of 8.5 (·····), 7.4 (——), or 6.5 (– – –). (*B*) Corresponding measurements from the same cells as shown in *A*, using voltage steps from a prepotential of −85 mV to a clamp potential of −45 mV. (*C*) Dependence of time constants on pH_i: open symbols show mean values ± SD from deactivation time constants (n = 4); closed symbols are mean values ± SD of activation time constants (n = 4). Fast time constants (τ_{a1}, fast activation time constant; τ_{d1}, fast deactivation time constant) are shown by squares, and slow time constants (τ_{a2}, τ_{d2}) are shown by circles. (*D*) Dependence of deactivation time constants on the Cl^- gradient shown as calculated Cl^- equilibrium potential (E_{Cl}). For each tested Cl^- gradient or pH_i, mean values of time constants at test potentials between −145 mV and −75 mV (deactivation) or between −75 mV and −25 mV (activation) were averaged from at least four cells. These mean values are then plotted versus pH_i or E_{Cl}. (*E*) Dependence of the relative late current (I_{ss}/I_{peak}) on E_{Cl}. Values were obtained by determining the limiting value of *C* for hyperpolarizing potentials from measurements shown in Fig. 1 *A*. (*F*) Variation of k_{on} and k_{off} with E_{Cl}, k_{on}, and k_{off} are rate constants connecting the open and the closed state in the fast deactivating kinetic state. In *D–F*, E_{Cl} was calculated from the internal and external Cl^- concentrations given in *D*.

nels will be nondeactivating, thus accounting for the increased constant term. If the voltage sensor had more than one charged residue, external acidification would result in a decrease in the gating charge of a fraction of the channels. A reduction of the equivalent gating charge would cause an increase in the slope factor of the activation curves and would have been easily recognized.

The chemical nature of the residue involved in voltage sensing can be inferred from the effect of extracellular acidification. These data are most consistent with a residue existing in a charged state at neutral and alkaline pH_e, but in an uncharged state at acid pH_e. This implicates amino acid residues with a carboxylic acid side group that are negatively charged at neutral pH. The data presented in Fig. 7 demonstrate at least 1.7 titratable groups in the channel. Because each voltage sensor consists of a single titratable group, this number equals the number of voltage sensors per channel. In view of our earlier work to characterize the D136G mutation in hClC-1 (Fahlke et al., 1995), we feel that an aspartic acid residue in the first transmembrane segment of the channel is a strong candidate for an hClC-1 voltage sensor described by our model. The Boltzmann slope factors (k_V) obtained from the fits shown in Fig. 1 *D* provide an estimate of the product of charge and extent of movement of the proposed voltagesensors. Based on a single charge per voltage sensor model, most of the k_V values presented in Table 1 are consistent with the movement of the voltage sensing structure across the entire membrane electric field. One k_V value (13.4 ± 1.4 mV) derived from the fit of the slow deactivating fractional current component does not agree with this notion. The mathematical complexity of this data fit ($2B^*[1 - B]$) requiring five parameters may not be as reliable as the fast and nondeactivating components, which require only three fit parameters for the same number of data points.

ClC channels are believed to be multimeric (Steinmeyer et al., 1994; Middleton et al., 1994). Our data are most consistent with a homodimeric channel complex in which each subunit contributes one voltage sensor. They do not rule out the possibility of tetrameric channel complexes

with two identical "protochannels." In the case of a tetrameric channel with a single pore, in half of the subunits, the voltage sensing residue would have to be immobilized by some unknown mechanisms.

A cytoplasmic gate in hClC-1

Our model also proposes the existence of a final blocking-unblocking step analogous to the "ball and chain" mechanism that operates in voltage-gated Na^+ and K^+ channels (Armstrong and Bezanilla, 1977; Hoshi et al., 1990; Demo and Yellen, 1991). In hClC-1, this blocking mechanism appears to interact with the ion pore, as evidenced by the effect of Cl^- ions on the rate constants derived for this blocking step (Fig. 7 *F*). Furthermore, in view of the profound effect of pH_i on the time constants of deactivation and activation (Fig. 7 *C*), it seems likely that the channel is blocked from the cytoplasmic side of the membrane. The dependence of k_{on} on the Cl^- gradient further indicates that the cytoplasmic gate may be competing with Cl^- ions for a common binding site, and indirectly suggests that the gate is negatively charged. The effect of permeating ions on the blocking-unblocking process in hClC-1 differs from the well-investigated examples of charybdotoxin block of Ca^{2+}-activated K^+ channels (MacKinnon and Miller, 1988) and the interaction of the inactivation ball with *Shaker* potassium channels (Demo and Yellen, 1991), in which permeating ions on the opposite side of the membrane were reported to knock out the blocking particle. In hClC-1, unbinding of the blocking particle is not affected by external or internal Cl^- concentration (k_{off}, Fig. 8 *F*). Nevertheless, the dependence of the rate constant k_{on} on the internal as well as the external Cl^- concentration clearly supports the idea that the cytoplasmic gate of hClC-1 channels is interacting with the ion conduction pathway. The observed voltage-dependent variation in the relative numbers of channels in the fast deactivating, slow deactivating, and nondeactivating states can be explained by an ultrafast voltage-induced conformational change mediated by the voltage sensors that alters the on rate of the blocking particle. This very rapid conformation change precedes the opening and closing transitions, and this helps to explain the observed voltage independence of activation and deactivation time constants. Alternative explanations for the voltage-independent gating kinetics include the location of the cytoplasmic gate outside of the membrane electric field, or the fact that the blocking particle is uncharged but interacts with a charged docking site on the channel.

Our data indicate that final opening and closing transitions are mediated by a cytoplasmic gate and not by the voltage sensor itself. In the absence of single-channel data on ClC-1, it is unknown whether the different configurations of the voltage sensor cause changes in the single-channel conductance of the channel. Further studies are necessary to address this question.

Comparison with the *Torpedo electroplax* Cl^- channel

ClC-0, the chloride channel of the electric organ of *Torpedo*, is the only other channel of the ClC family for which the gating behavior has been quantitatively described. Although there is considerable sequence homology between hClC-1 and ClC-0 (54% amino acid identity), several functional differences exist that make the models developed for each of these two isoforms incompatible.

Based on experiments with planar lipid bilayers (White and Miller, 1979; Hanke and Miller, 1983; Richard and Miller, 1990), gating of ClC-0 was described by the function of two different "gates": a fast gate activated upon membrane depolarization, and a slow gate operating during hyperpolarization. The coexistence of these two different processes gives rise to a distinct pattern of single-channel behavior ("double-barreled shotgun") in which two conductance states are independently opened and closed by the fast gate while the slow gate remains open. A slow gate has not been observed in muscle Cl^- channels (Steinmeyer et al., 1991b; Fahlke et al., 1995).

For ClC-0 channels expressed in *Xenopus* oocytes, the fast gate was reported to depend on the Cl^- gradient (Richard and Miller, 1990; Pusch et al., 1995). When the Cl^- equilibrium potential was experimentally shifted, the macroscopic activation of the fast gate changed in parallel. Based on this strong coupling between ion permeation and gating, the permeating ion was proposed to be the only gating charge (Pusch et al., 1995). In contrast, when shifts of E_{Cl} were performed with hClC-1, the activation curve was shifted in the opposite direction (Fahlke et al., 1995). Moreover, the D136G mutation causes dramatic differences in voltage-dependent gating, and its open probability is strictly coupled to the E_{Cl}. These two observations, together with the absence of significant changes in pore properties, indicate the existence of a voltage sensor as part of the protein sequence that is disabled in the D136G mutation (Fahlke et al., 1995).

A coupling between E_{Cl} and the activation curve in ClC-0 (Pusch et al., 1995) does not exclude the existence of a voltage sensor. The Cl^- concentration on both sites of the membrane may influence the position of a negatively charged voltage sensor that interacts electrostatically with anions at a binding site within the channel. Whether the activation curve shifts in parallel with E_{Cl} or in the opposite direction depends on the relative positions of the Cl^- binding site and the voltage sensor.

In WT hClC-1, lowering the external Cl^- concentration causes a shift of the activation curve in the direction opposite to the change in E_{Cl}. Several explanations exist for this effect (Hals and Palade, 1990). If the impermeant anion ($CH_3SO_3^-$ in our experiments) would bind to the outer vestibule with longer residency time than Cl^- and electrostatically interact with the negatively charged voltage sensor, then an increase in extracellular $CH_3SO_3^-$ concentration would result in a leftward shift of the

voltage dependence, as observed. This explanation is also valid for the effect of external iodide on the gating properties of hClC-1 (Fahlke and George, manuscript in preparation).

The molecular mechanisms responsible for the differences between ClC-0 and ClC-1 with respect to the gating effects of the permeating ion are unclear. The functional effect of neutralizing D70, the residue in ClC-0 corresponding to the proposed voltage sensor D136 in hClC-1, is currently unknown (Pusch et al., 1995).

SUMMARY

Based on macroscopic current recordings, we propose a model for the gating of hClC-1 channels that explains the activation and deactivation of macroscopic currents for variable intracellular and extracellular pH and Cl^- concentration. We postulate that a set of two identical single negatively charged residues function as voltage sensors. The two voltage sensors may assume three different conformations, each of which confers a unique kinetic state. As a consequence, current activation as well as deactivation consist of three different components, with fast, slow, and time-independent time courses. The rearrangements that the two voltage sensors undergo with changing membrane potential are very rapid.

This model is able to explain the principal macroscopic gating properties described so far for hClC-1: 1) the occurrence of three current components, the fractional amplitudes of which are highly voltage dependent; 2) the identity of the fast deactivation and activation time constants; 3) the behavior of the channel with varied internal and external pH; and 4) the effect of different Cl^- gradients on activation and deactivation time constants. There are, of course, several open questions. We do not know whether the different kinetic states correspond to different conductance states. In addition, the molecular nature of the voltage sensors and of the cytoplasmic gate is not completely understood.

We would like to thank Dr. Richard Horn and Dr. Paul Bennett for their critical review of the manuscript. We also thank Ms. Traudl Hiller, Ms. Margit Rudolph, and Ms. Sigrun Schäfer for their excellent technical assistance, and Ms. Ursula Pika for invaluable help with the cell transfection.

Supported by the DFG (Ru 138/17-3 and Fa 301/1-1), the Muscular Dystrophy Association, and the Lucille P. Markey Charitable Trust. ALG is a Lucille P. Markey Scholar.

REFERENCES

Adachi, S., S. Uchida, H. Ito, M. Hata, M. Hiroe, F. Marumo, and S. Sasaki. 1994. Two isoforms of a chloride channel predominantly expressed in thick ascending limb of Henle's loop and collecting ducts of rat kidney. *J. Biol. Chem.* 269:17677–17683.

Almers, W. 1978. Gating currents and charge movements in excitable membranes. *Rev. Physiol. Biochem. Pharmacol.* 82:96–190.

Armstrong, C. M., and F. Bezanilla. 1977. Inactivation of the sodium channel. II. Gating current experiments. *J. Gen. Physiol.* 70:567–590.

Brown, A. M., Y. Tsuda, and D. L. Wilson. 1983. A description of activation and conduction in calcium channels based on tail and turn-on current measurements in the snail. *J. Physiol. (Lond.).* 344:549–583.

Chiu, S. Y. 1977. Inactivation of sodium channels: second order kinetics in myelinated nerve. *J. Physiol. (Lond.).* 273:573–596.

Demo, S. D., and G. Yellen. 1991. The inactivation gate of the *Shaker* K^+ channel behaves like an open-channel blocker. *Neuron.* 7:743–753.

Fahlke, Ch., and R. Rüdel. 1995. Chloride currents across the membrane of mammalian skeletal muscle fibres. *J. Physiol. (Lond.).* 484:355–368.

Fahlke, Ch., R. Rüdel, N. Mitrovic, M. Zhou, and A. L. George, Jr. 1995. An aspartic acid residue important for voltage-dependent gating of human muscle chloride channels. *Neuron.* 15:463–472.

George, A. L., M. A. Crackower, J. A. Abdalla, A. J. Hudson, and G. C. Ebers. 1993. Molecular basis of Thomsen's disease (autosomal dominant myotonia congenita). *Nature Genet.* 3:305–310.

Graham, R. L., and A. J. van der Eb. 1973. A new technique for the assay of infectivity of human adenovirus 5 DNA. *Virology.* 52:456–467.

Hals, G. D., and P. T. Palade. 1990. Different sites control voltage dependence and conductance of sarcoball anion channel. *Biophys. J.* 57: 1037–1047.

Hamill, O. P., A. Marty, E. Neher, B. Sakmann, and F. J. Sigworth. 1981. Improved patch-clamp techniques for high-resolution current recording from cells and cell-free membrane patches. *Pflügers Arch.* 391:85–100.

Hanke, W., and C. Miller. 1983. Single chloride channels from *Torpedo electroplax.* Activation by protons. *J. Gen. Physiol.* 82:25–45.

Hoshi, T., W. N. Zagotta, and R. W. Aldrich. 1990. Biophysical and molecular mechanisms of *Shaker* potassium channel inactivation. *Science.* 250:533–538.

Jentsch, T. J., K. Steinmeyer, and G. Schwarz. 1990. Primary structure of *Torpedo* marmorata chloride channel isolated by expression cloning in Xenopus oocytes. *Nature.* 348:510–514.

Kawasaki, M., S. Uchida, T. Monkawa, A. Miyawaki, K. Mikoshiba, F. Maruma, and S. Sasaki. 1994. Cloning and expression of a protein kinase C-regulated chloride channel abundantly expressed in rat brain neuronal cells. *Neuron.* 12:597–604.

Koch, M. C., K. Steinmeyer, C. Lorenz, K. Ricker, F. Wolf, M. Otto, B. Zoll, F. Lehmann-Horn, K. H. Grzeschik, and T. J. Jentsch. 1992. The skeletal muscle chloride channel in dominant and recessive human myotonia. *Science.* 257:797–800.

Liman, E. R., P. Hess, F. Weaver, and G. Koren. 1991. Voltage-sensing residues in the S4 region of a mammalian K^+ channel. *Nature.* 353: 752–776.

Logothetis, D. E., S. Movahedi, C. Satler, K. Lindpaintner, and B. Nadal-Ginard. 1992. Incremental reductions of positive charge within the S4 region of voltage-gated K^+ channel result in corresponding decreases in gating charge. *Neuron.* 8:531–540.

MacKinnon, R., and C. Miller. 1988. Mechanism of charybdotoxin block of the high-conductance Ca^{2+}-activated K^+ channel. *J. Gen. Physiol.* 91:335–349.

Middleton, R. E., D. J. Pheasant, and C. Miller. 1994. Purification, reconstitution, and subunit composition of a voltage-gated chloride channel from *Torpedo electroplax. Biochemistry.* 33:13189–13198.

Papazian, D. M., L. C. Timpe, Y. N. Jan, and L. Y. Jan. 1991. Alteration of voltage-dependence of *Shaker* potassium channel by mutations in the S4 sequence. *Nature.* 349:305–310.

Pusch, M., U. Ludewig, A. Rehfeldt, and T. J. Jentsch. 1995. Gating of the voltage-dependent chloride channel ClC-0 by the permeant anion. *Nature.* 373:527–530.

Pusch, M., K. Steinmeyer, and T. J. Jentsch. 1994. Low single channel conductance of the major skeletal muscle chloride channel, ClC-1. *Biophys. J.* 66:149–152.

Richard, E. A., and C. Miller. 1990. Steady-state coupling of ion-channel conformations to a transmembrane ion gradient. *Science.* 247: 1208–1210.

Steinmeyer, K., R. Klocke, C. Ortland, M. Gronemeier, H. Jockusch, S. Grunder, and T. J. Jentsch. 1991a. Inactivation of muscle chloride

channel by transposon insertion in myotonic mice. *Nature.* 354: 304–308.

Steinmeyer, K., C. Lorenz, M. Pusch, M. C. Koch, and T. J. Jentsch. 1994. Multimeric structure of ClC-1 chloride channel revealed by mutations in dominant myotonia congenita. *EMBO. J.* 13:737–743.

Steinmeyer, K., C. Ortland, and T. J. Jentsch. 1991b. Primary structure and functional expression of a developmentally regulated skeletal muscle chloride channel. *Nature.* 354:301–304.

Stühmer, W., F. Conti, H. Suzuki, X. Wang, M. Noda, N. Yahagi, H. Kubo, and S. Numa. 1989. Structural parts involved in activation and inactivation of the sodium channel. *Nature.* 339:597–603.

Thiemann, A., S. Grunder, M. Pusch, and T. J. Jentsch. 1992. A chloride channel widely expressed in epithelial and non-epithelial cells. *Nature.* 356:57–60.

Uchida, S., S. Sasaki, T. Furukawa, M. Hiraoka, T. Imai, Y. Hirata, and F. Marumo. 1993. Molecular cloning of a chloride channel that is regulated by dehydration and expressed predominantly in kidney medulla. *J. Biol. Chem.* 268:3821–3824.

van Siegtenhorst, M. A., M. T. Bassi, G. Borsani, M. C. Wapenaar, G. B. Ferrero, L. de Concillis, E. I. Rugarli, A. Grillo, B. Franco, H. Y. Zoghbi, and A. Ballabio. 1994. A gene from the Xp22.3 region shares homology with voltage-gated chloride channels. *Hum. Mol. Genet.* 3:547–552.

Vaughan, P., J. M. Kootsey, and M. D. Feezor. 1991. Kinetic analysis of chloride conductance in frog skeletal muscle at pH 5. *Pflügers Arch.* 419:522–528.

Warner, A. E. 1972. Kinetic properties of the chloride conductance of frog muscle. *J. Physiol. (Lond.).* 227:291–312.

White, M. M., and C. Miller. 1979. A voltage-gated anion channel from the electric organ of *Torpedo californica. J. Biol. Chem.* 254: 10161–10166.